J Electroceram (2012) 28:240–245
DOI 10.1007/s10832-012-9719-2

# A hysteresis model based on ellipse polar coordinate and microscopic polarization theory

**Changhai Ru · Tao Chen**

Received: 19 June 2011 / Accepted: 22 March 2012 / Published online: 15 April 2012


**Abstract** In this paper, the underlying anhysteretic polarization is derived based on Boltzmann statictics and Langevin model. The remnant polarization and the irreversible polarization are analyzed. A thermodynamic description of ferroelectric phenomena is proposed to address the coupling relationship between electrical field and mechanical field by considering the series expansion of the elastic Gibbs energy function. A simple linear mapping hysteresis model based on theory of microscopic polarization and ellipse polar coordinate is derived. In order to evaluate the effectiveness of the proposed model, a nano-positioning stage driven by the PZT in open-loop operation is used to test. The experimental results show that the proposed hysteresis model could precisely describe hysteresis phenomena. The model max relative error of full span range is about 0.5 %. The proposed model simplifies the identification procedure of its inverse model. It is experimentally demonstrated that the tracking precision is significantly improved.

**Keywords** Piezoelectric actuator · Hysteresis · Microscopic polarization · Linear mapping

## 1 Introduction

Piezoelectric actuators have become underlying components of a variety of positioning and sensing instruments in micro/nano scale applications. However, one of the drawbacks of the piezoelectric actuator is the existence of hysteresis. Without modeling and incorporating hysteresis in the controller design, hysteresis often severely limits system performance such as giving rise to undesirable inaccuracies or oscillations, even leading to instability [1]. Therefore, it is necessary to find a model to describe the behavior of hysteresis, and the corresponding controller based on the proposed hysteresis model is designed to eliminate the harmful effect of hysteresis.

In general, modeling approaches for hysteresis nonlinearity are classified into phenomenological and constitutive categories. Phenomenological models are formed based on pure mathematical basis. Phenomenological approaches for hysteresis modeling have also been developed extensively [2–9], such as Preisach operator [2, 3], KP hysteron model [4, 5], the Bouc–Wen model and the Prandtl-Ishlinskii operator [7–9]. Although the models provide a purely mathematical tool for modeling complex hysteresis loops, it does not provide a physical insight into the phenomenon. A variety of research works have been conducted for the constitutive approach. Aderiaens proposed an electromechanical model of piezoelectric actuators combined with nonlinear first order differential equations [10]. A generalized Maxwell resistive capacitor model was utilized as a lumped-parameters casual representation of hysteresis [11]. A descriptive set of memory-based properties had been proposed and validated for hysteresis nonlinearity through extensive experiments on piezoelectric actuators [12]. However, the major drawback of these approaches is the limited accuracy due to the lack of understanding the underlying nature of the hysteresis phenomenon and can not explain why voltage-controlled mode will result in hysteresis. In this paper, the remnant polarization and the irreversible polarization are analyzed and a thermodynamic description of

C. Ru (✉)
College of Automation, Harbin Engineering University,
Harbin, China 150001
e-mail: rchhai@gmail.com

C. Ru · T. Chen
Centre of Robotics and Microsystem, Soochow University,
Soochow, China 215021

ferroelectric phenomena is proposed to address the coupling relations between electrical field and mechanical field by considering the series expansion of the elastic Gibbs energy function. Finally, a simple linear mapping hysteresis model based on the theory of microscopic polarization is derived and tested.

## 2 Microscopic polarization model

For a dipole moment $\mathbf{P_0}$ in an electric field $\mathbf{E}$, the potential energy is given by

$$u = -\mathrm{P}_0 \cdot \mathrm{E} = -p_0 E\cos\theta \tag{1}$$

where $p_0 = |\mathrm{P}_0|$, $E = |\mathrm{E}|$ and $\cos\theta$is the direction cosines between polarization and electric field. Classical Boltzmann statistics can be used to express the probability of dipoles occupying energy states. $k$ is denoted Boltzmann's constant, the thermal energy is $kT$ and the probability that a dipole occupies the energy state $u$ is

$$\mu(\varepsilon) = Ce^{-\varepsilon/kT} \tag{2}$$

The parameter $C$ is later specified to ensure that integration over all possible configurations yields the total number of moments per unit volume $N$.

Under the assumption of an isotropic material, the number of moments between $\theta$and $\theta$+$d\theta$ are proportional to the surface area $2\pi\sin\theta d\theta$ on a unit sphere. With the probability of occupying the state given by Eq. (2), the number of moments in this configuration can be expressed

$$dN = 2\pi\sin\theta d\theta C e^{p_0 E\cos\theta/kT} \tag{3}$$

To evaluate $C$, the integration of $dN$ over all possible configurations must equal the total number of moments per unit volume $N$. So

$$C = \frac{N}{2\pi\int_0^\pi e^{p_0 E\cos\theta/kT}\sin\theta d\theta} = \frac{N}{\frac{4\pi kT}{p_0 E}\sinh(\frac{p_0 E}{kT})} \tag{4}$$

Langevin model is given.

$$P = Np_0[\coth(\frac{p_0 E}{kT}) - \frac{kT}{p_0 E}] = Np_0 L(\frac{p_0 E}{kT}) \tag{5}$$

where the $L$ is Langevin function,

$$L(x) = \coth(x) - \frac{1}{x} \tag{6}$$

Then the polarization can be expressed as

$$P = N\cdot\frac{p_0^2}{3kT}\lambda(E)\cdot E\,\lambda(E) = 1 - \frac{1}{15}E + \cdots \tag{7}$$

In an isotropic dielectric material, the induced polarization is given by

$$P = \chi\varepsilon_0 E \tag{8}$$

where $\varepsilon_0$ is the permittivity of free space and is nonlinear susceptibility. According to Eq. (7), the $\chi$ is given by

$$\chi = \frac{N}{\varepsilon_0}\cdot\frac{p_0^2}{3kT}\lambda(E) \tag{9}$$

From Eqs. (7) and (9), the polarization $P$ and electric field have a nonlinearity relation and the susceptibility $\chi$ is a nonlinear function about electric field $E$.

The energy required to break the pinning sites and move the domain wall is

$$u_{pin}(P) = -\delta\int_0^P dP \tag{10}$$

where $\delta = \frac{n<u_\pi>}{2p}$, and $n$ denotes the average density of pinning sites and $<u_\pi>$ denotes the average energy for $180^\circ$ domain walls.

To quantify the irreversible polarization process, the work required to attain a specified polarization level should be determined. The work is

$$w = \frac{1}{\varepsilon_0}\int_0^{\mathrm{D}} \mathrm{P}\cdot d\mathrm{D} \tag{11}$$

where $\mathbf{D}$ is electric displacement.

$$\frac{dP_{irr}}{dE} = \frac{(P_{an} - P_{irr})}{\delta - (P_{an} - P_{irr})/\varepsilon_0}. \tag{12}$$

where $P_{irr}$ denotes the irreversible polarization and $P_{an}$ is the anhysteretic polarization given by Eq. (7). Equation (12) is the microscopic polarization model considering the domain wall theory. The ideal polarization $P_{an}$ and the coefficient $\delta$ are the function of electric field. Hence the irreversible polarization $P_{irr}$ is also the function of electric field. But it shows hysteresis relationship between $P_{irr}$ and $E$ due to the energy loss of domain wall movement. It is difficult to solve the $P_{irr}$ according to Eq. (12). The inequation $P_{irr} < P_{an}$ is correct because of the energy loss. For the further derivation, $P_{irr}$ and $E$ have the analogous relation with Eq. (8)

$$P_{irr} = \chi'\varepsilon_0 E \tag{13}$$

$$\chi' = \frac{N}{\varepsilon_0}\cdot\frac{p_0^2}{3kT}\lambda'(E) \tag{14}$$

where $\chi$' is the irreversible susceptibility considering the energy loss of domain wall movement and $\lambda$'($E$) is a polynomial about $E$.

Piezoelectric ceramic belongs to ferroelectric materials, which had been prepolarized by a high electric field. When the

high electric field is removed, the polarization is not zero, which is defined as the remanent polarization $P_r$. The electric is called the coercive field $E_C$ when the polarization is zero. The $P$ versus $E$ curve is illustrated in Fig. 1. $P_S$ is the spontaneous polarization of piezoelectric ceramic. Rectangle section is the working range of piezoelectric actuator under positive input voltage.

The total polarization $P$ is the sum of the irreversible polarization $P_{irr}$ and remnant polarization $P_r$.

$$P = P_r + P_{irr} \tag{15}$$

$P_r$ is assumed to be reversible when the applied stress is zero. By considering the series expansion of the elastic Gibbs energy function in one-dimension, the thermodynamic description of ferroelectric phenomena is obtained

$$G_1(P, X, T) = \frac{T - T_0}{2C}P^2 + \frac{1}{4}\beta P^4 + \frac{1}{6}\gamma P^6 - \frac{1}{2}sX^2 - GP^2X$$

where $T_0$ is Curie-Weiss temperature, T is the temperature, C is Curie constant, $\beta$ and $\gamma$ are the coefficient , s is the elastic compliance, $X$ is the applied stress, and $G$ is the electrostriction coefficient. The strain $x$ is

$$x = -\frac{\partial G_1}{\partial X} = sX + GP^2 \tag{16}$$

When the applied stress is zero, Eq. (16) becomes

$$x = G(P_r + P_{irr})^2 = GP_r^2 + gP_{irr} + GP_{irr}^2 \tag{17}$$

$$x = G(P_r + \chi'\varepsilon_0 E)^2 = GP_r^2 + dE + ME^2 \tag{18}$$

where the piezoelectric strain coefficient $g$ ($m^2/C$) may be expressed as

$$g = 2GP_r \tag{19}$$

G is the electrostriction coefficient ($m^4/C^2$). $d$ is the piezoelectric coefficient (m/V), and can be expressed as:

$$d = 2\chi'\varepsilon_0 GP_r \tag{20}$$

M is the electrostriction coefficient ($m^2/V^2$).

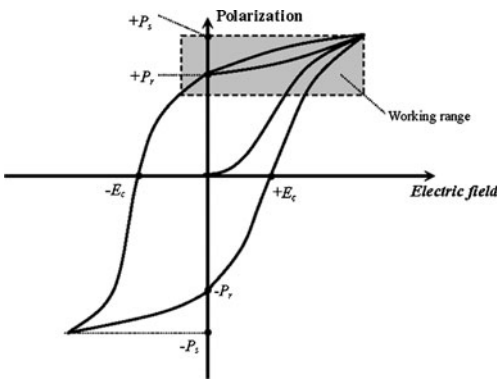


**Fig. 1** Hysteresis loop *of polarization* VS. *electric field*

## 3 A linear mapping hysteresis model based on polarization theory

If the electric field is selected as the control variable, the contributions of electric field to the strain include three parts according to Eqs. (17) and (18).

**The part one:** the remnant polarization strain which is reversible without hysteresis is given by

$$x_r = GP_r^2 \tag{21}$$

Commonly, the strain $x$ of piezoelectric actuator is the deformation based on the remnant polarization strain $x_r$.

**The part two:** the piezoelectric strain is given by

$$x_{irr} = dE = gP_{irr} \tag{22}$$

If the strain of piezoelectric material is controlled by electric field $E$, the relation between $x_{irr}$ and $E$ shows hysteresis because the piezoelectric strain coefficient $d$ is variant and related to electric field $E$ according to Eqs. (20) and (14). However, it is different to the control method based on electric polarization. The strain of piezoelectric material has a linear relationship between $x_{irr}$ and $P_{irr}$ because the piezoelectric strain coefficient $g$ has nothing to do with the electric field E according to Eq. (19). So there will be no hysteresis theoretically.

**The part three:** the electrostriction strain is given by

$$x_k = GP_{irr}^2 = ME^2 \tag{23}$$

From Eq. 23, we can see that the electrostriction strain is expressed by $P_{irr}$ and $E$ respectively. Although G and M are both called electrostriction coefficient, the dimensions of the quantity are different. The piezoelectric ceramics are prepolarized. Compared with that of piezoelectric inverse effect, the contribution of electrostriction effect can be ignored.

According to the Eq. 22, the piezoelectric strain $x$ is

$$x(u) = \frac{L(u)}{L} = g \cdot P(u) \tag{24}$$

where $L(u)$ is the deformation of piezoelectric actuator, $L$ is the length of piezoelectric actuator, $P$ is the irreversible polarization based on the remnant polarization $P$ (Omit the subscript 'irr' for convenience) and $u$ is the external driving voltage.

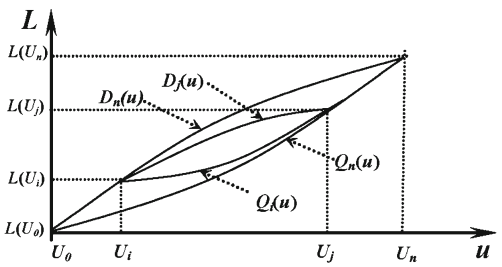


**Fig. 2** Hysteresis curves of displacement $L$ vs. voltage $u$

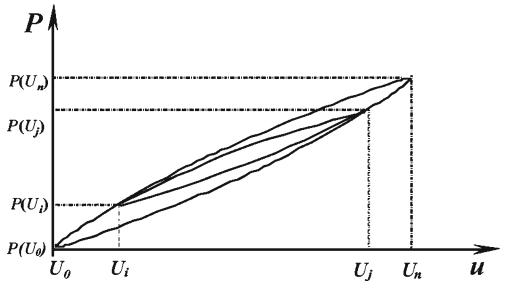


**Fig. 3** Hysteresis curves of polarization $P$ vs. voltage $u$

It is linear relation relationship between $L$ and $P$.

$$L(u) = gL \cdot P(u) \tag{25}$$

Hysteresis trajectory starts moving on the ascending curve which passes through the initial point, as schematically depicted in Fig. 2. This curve could be approximated by a monotonically increasing continuous function $Q_n(u)$ which is called the referenced ascending curve, and the voltage $U_i$ is called as turning voltage. The $U_i$ value decides the direction of input control voltages and shapes of hysteresis curves, and is random and different in different operation process. The range of turning voltage is from the initial voltage $U_0$ to the convergent voltage $U_n$. The any raising loading curves which start from the $U_i$ are called as raising hysteresis curves $Q_i(u)$. If the direction of input voltages changes immediately after reaching its maximum allowed value $U_n$, the hysteresis trajectory breaks its path and moves downward on the descending loading curve, which can be approximated by another monotonically increasing continuous function $D_n(u)$, which is called as the referenced descending curve and the voltage $U_j$ is also named turning voltage. The any descending loading curves which begin from the point $U_j$ are named descending hysteresis curves $D_j(u)$.

If the piezoelectric actuator is driven by the initial voltage $U_0$ or the maximum voltage $U_n$. The polarizations are $P(U_0)$ and $P(U_n)$ respectively. According to the Eq. 25, the output displacements are

$$\begin{cases} L(U_0) = gL \cdot P(U_0) \\ L(U_n) = gL \cdot P(U_n) \end{cases} \tag{26}$$

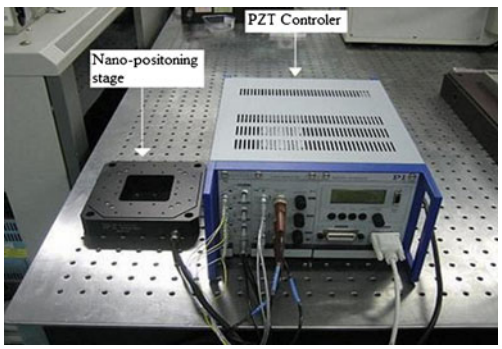


**Fig. 4** The experimental equipments

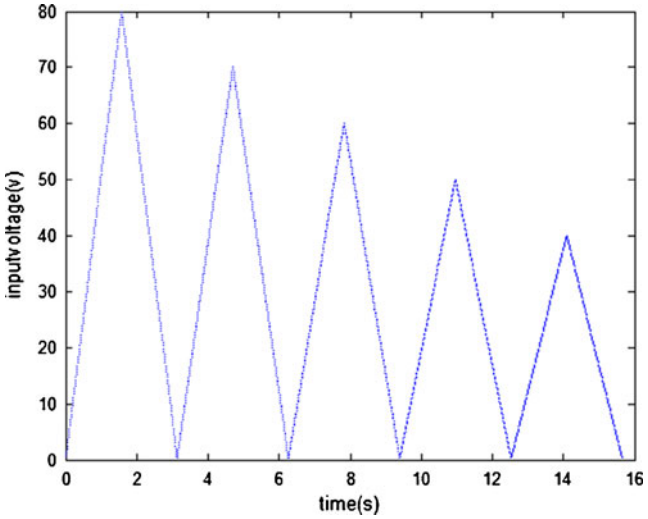


**Fig. 5** The applied voltage on piezoelectric actuator

Hysteresis trajectory starts moving along the referenced ascending curve $Q_n(u)$. If the direction of input voltage changes at any turning voltage $U_j$, and moves downward on the referenced descending curve $D_n(u)$. Then direction of input voltage changes again at turning voltage $U_i$. The relationship between polarization $P$ and voltage $u$ is shown in Fig. 3. The output displacements at the turning points $U_i$ and $U_j$ are

$$\begin{cases} L(U_i) = gL \cdot P(U_i) \\ L(U_j) = gL \cdot P(U_j) \end{cases} \tag{27}$$

The relation equations at different turning voltage are

$$\begin{cases} L(U_i) = k_1 \cdot L(U_0) \\ L(U_j) = k_2 \cdot L(U_n) \end{cases} \begin{cases} k_1 = P(U_i)/P(U_0) \\ k_2 = P(U_j)/P(U_n) \end{cases} \tag{28}$$

The all points of raising hysteresis curve $Q_i(u)$ in interval $[U_i, U_j]$ can find their linear mapping points in referenced

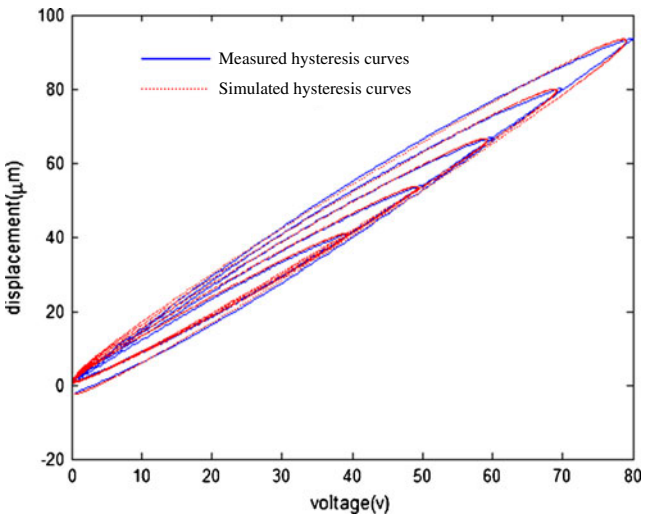


**Fig. 6** The simulated curves and measured curves

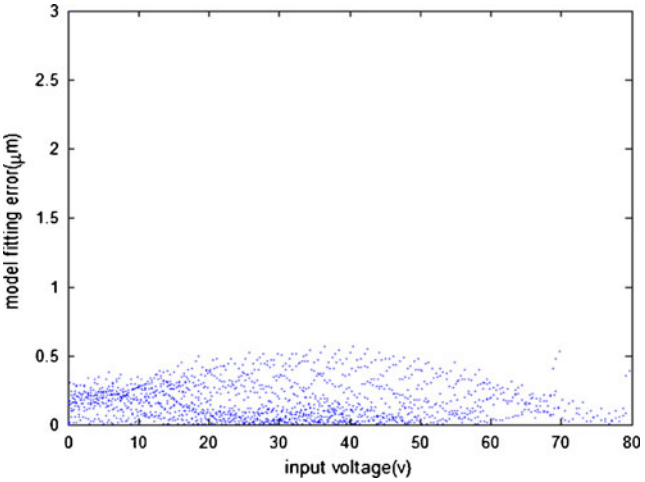


**Fig. 7** The model fitting errors

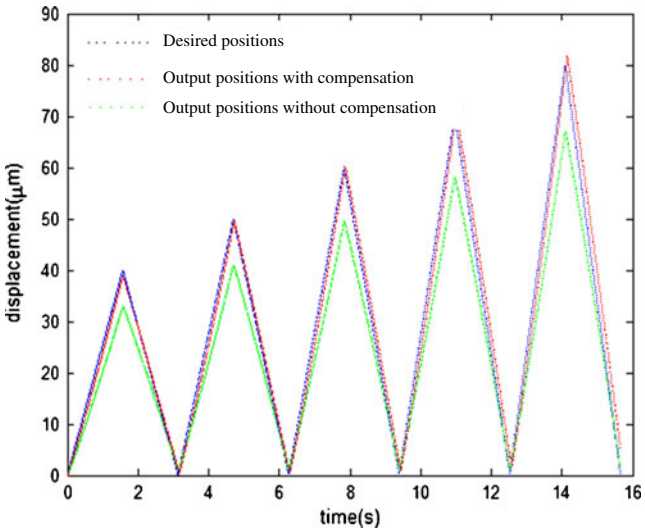


**Fig. 9** Output response with and without hysteresis compensation

ascending curve $Q_n(u)$ in interval $[U_0, U_j]$. Analogously, the all points of descending hysteresis curve $D_i(u)$ in interval $[U_i, U_j]$ can find their linear mapping points in referenced ascending curve $D_n(u)$ in the interval $[U_i, U_n]$. Therefore, if the referenced raising curve and the referenced descending curve are obtained, the rest of internal hysteresis curves are also obtained through the linear mapping strategy. So a method can be established to describe all raising and descending curves.

Ellipse polar coordinate is applied in the hysteresis model, which has the advantage that the proposed model simplifies the identification procedure of its inverse model. $\alpha$ is the parameter of ellipse polar coordinate.

For $u > U_j$, the ascending curves model is

$$\begin{cases} L(u) = Q_i(\alpha) = a_i \sin(\theta_i)\cos(\alpha) + b_i \cos(\theta_i)\sin(\alpha) + q_{0i} \\ u(\alpha) = a_i \cos(\theta_i)\cos(\alpha) + b_i \sin(\theta_i)\sin(\alpha) + u_{0i} \\ q_{0i} = \dfrac{L(U_i) + L(U_n)}{2}, u_{0i} = \dfrac{U_i + U_n}{2}, \theta_i = \arctan\left(\dfrac{L(U_n) - L(U_i)}{U_n - U_i}\right) \\ a_i = \dfrac{\sqrt{(L(U_n) - L(U_i))^2 + (U_n - U_i)^2}}{2} b_i = a_i \dfrac{b_1}{a_1} \end{cases} \tag{29}$$

For $u < U_j$, the descending curves model is

$$\begin{cases} L(u) = D_i(\alpha) = a_i' \sin(\theta_i')\cos(\alpha) + b_i' \cos(\theta_i')\sin(\alpha) + d_{0i} \\ u(\alpha) = a_i' \cos(\theta_i')\cos(\alpha) + b_i' \sin(\theta_i')\sin(\alpha) + u_{0i}' \\ d_{0i} = \dfrac{L(U_j) + L(U_0)}{2}, u_{0i}' = \dfrac{U_j + U_0}{2}, \theta_i' = \arctan\left(\dfrac{L(U_j) - L(U_0)}{U_j - U_0}\right) \\ a_i' = \dfrac{\sqrt{(L(U_j) - L(U_0))^2 + (U_j - U_0)^2}}{2} b_i' = a_i' \dfrac{b_1'}{a_1'} \end{cases} \tag{30}$$

where $L(u)$ is the output displacement of piezoelectric actuator, the parameters $a_i, a_i', b_i, b_i', \theta_i, \theta_i', q_{0i}, d_{0i}, , u_{0i}, u_{0i}'$ are the coefficients of the proposed hysteresis model, which can be obtained according to different turning voltage $U_i$ or $U_j$. The $a_1, b_1, a_1', b_1'$ is the polar coordinate parameters of the referenced curves $Q_n(u)$ and $D_n(u)$, which are obtained according to the experimental data of the input control voltages and displacements. The recursive least squares(RSL) identification algorithms is used for the model identification [13].

## 4 Experimental setup and model verification

To evaluate the quality of the new hysteresis model, a nano-positioning system driven by the PZT was used for test. Figure 4 illustrates the test and measure equipments of the experiment. It consists of a computer (digital signal processor) that generates the desired position signals and implements the control procedure for the piezoelectric actuator. The nano-positioning stage is P-517.3CL XYZ Piezo Nano-positioning Stage from PI Corp., whose travel ranges are 100 μm, 100 μm and 20 μm in X, Y, Z axis respectively. The actual output displacements of the piezoelectric actuator are measured by the Capacitive Displacement Sensor in PZT Controller and converted to a digital signal.

For convenient use, in the process of fitting, all the experimental displacement values are normalized at first, after model fitting, the fitting data are transforated according to relevant magnification and initial value. The nano-positioner is excited by the decreasing triangular voltages in Fig. 5 under open-loop operation. The measured hysteresis curves with blue lines and the simulated hysteresis

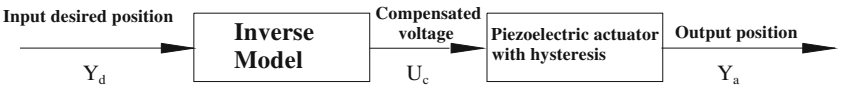


**Fig. 8** Inverse control structure diagram

curves with red dotted lines are shown in Fig. 6. A very good agreement is exhibited between simulations and measurements, which demonstrates that the proposed hysteresis model could precisely describe hysteresis phenomena. The model fitting errors are less than 0.5 μm as shown in Fig. 7. The max relative error of full span range is about 0.5 %.

Figure 8 shows the structure diagram of inverse control compensation controller in an open-loop operation. To implement an open-loop control scheme for tracking a desired position, the inverse controller maps the desired position $Y_d$ into a compensated voltage $U_c$. The actual output position $Y_a$ will follow the desired signal $Y_d$.

The hysteresis model makes use of polar coordinate which has the advantage that the proposed model simplifies the identification procedure of its inverse model to a large extent. The inverse model is given as following.

The inverse of ascending curve model is

$$\begin{cases} Y_d = a_i \cos(\theta_i)\cos(\alpha) + b_i \sin(\theta_i)\sin(\alpha) + u_{0i} \\ U_c = a_i \sin(\theta_i)\cos(\alpha) + b_i \cos(\theta_i)\sin(\alpha) + q_{0i} \end{cases} \quad (31)$$

The inverse of descending curve model is

$$\begin{cases} Y_d = a_i' \cos(\theta_i')\cos(\alpha) + b_i' \sin(\theta_i')\sin(\alpha) + u_{0i}' \\ U_c = a_i' \sin(\theta_i')\cos(\alpha) + b_i' \cos(\theta_i')\sin(\alpha) + d_{0i} \end{cases} \quad (32)$$

The parameters $a_i, a_i', b_i, b_i', \theta_i, \theta_i', q_{0i}, d_{0i}, , u_{0i}, u_{0i}'$ are the coefficients of the proposed hysteresis model, which have been given before. The control effect by applying inverse model is shown in Fig. 9. The blue dotted line is the desired output positions. While the green dotted line is the actual output response of the piezoelectric actuator without hysteresis compensation. The red dotted line is the output response with hysteresis compensation. From Fig. 9, we can see that the output positions can track accurately the desired positions after compensating hysteresis. The hysteresis and nonlinearity between the output displacement and applied voltage is more obvious in open-loop operation when the voltage is increased. So it can be seen that the error increases by increasing the voltage without the hysteresis compensation.

## 5 Conclusions

The main contribution of this paper is to apply microscopic polarization mechanism and domain wall theory to explain hysteresis. This theory is based on the quantification of the reversible and irreversible motion of domain walls pinned. A thermodynamic description of ferroelectric phenomena is proposed to address the coupling relations between electrical field and mechanical field by considering the series expansion of the elastic Gibbs energy function. The reason why hysteresis can be reduced by controlling polarization is explained according to the analysis of microscopic polarization mechanism and domain wall theory. The reason of occurring hysteresis in voltage control mode is also given. Then a simple linear mapping hysteresis model based on microscopic polarization is derived. Finally, a nanopositioning stage driven by the PZT in open-loop operation is used to test. The experimental results show that the proposed hysteresis model could precisely describe hysteresis phenomena. The model fitting errors are less than 0.5 μm and the max relative error of full span range is about 0.5 %. It is experimentally demonstrated that the tracking precision is significantly improved based on the inverse model of proposed hysteresis model.

**Acknowledgements** The authors gratefully acknowledge financial support from the National Natural Science Foundation of China under Grant No. 61174087 and Foundation for University Key Teacher of Heilongjiang Province of China.

## References

1. G. Tao, P.V. Kolotovic, IEEE Trans. Autom. Control. **40**(2), 200 (1995)
2. P. Ge, M. Jouaneh, IEEE Trans. Control. Syst. Technol. **4**(3), 211 (1996)
3. P. Ge, M. Jouaneh, Precis. Eng. **20**, 99 (1997)
4. M.A. Krasnoskl'skii, A.V. Pokrovskii, (Springer-Verlag, New York, 1989)
5. G. Webb, A. Kurdila, D. Lagoudas, J. Guid. Control. Dyn. **23**(3), 459 (2000)
6. J. Ha, Y. Kung, R. Fung, Sensor Actuator Phys. **132**, 643 (2006)
7. K. Kuhnen, H. Janocha, *6th International Conference on New Actuators*, (Bremen, 1998), p. 309
8. P. Kreci, K. Kuhnen, IEE Proc. Contr. Theor. Appl. **148**(3), 185 (2001)
9. K. Kuhnen, H. Janocha, Sensor Actuator Phys. **79**, 83 (2000)
10. H. Aderiaens, W. Koning, R. Baning, IEEE ASME Trans. Mechatron. **5**, 331 (2000)
11. M. Goldfarb, N. Celanovic, ASME J. Dyn. Syst. Meas. Contr. **119**, 478 (1997)
12. S. Bashash, N. Jalili, J. Appl. Phys. **100**(1), 014103 (2006)
13. E. James, IEEE Trans. Automat. Contr. **38**, 351 (1993)